Single-mode lasers and parity-time symmetry broken gratings based on active dielectric-loaded long-range surface plasmon polariton waveguides

Choloong Hahn,[1] Seok Ho Song,[1] Cha Hwan Oh,[1] and Pierre Berini[2,3,4*]

[1]*Department of Physics, Hanyang University, 222 Wangsimni-ro, Seoul, South Korea*
[2]*School of Electrical Engineering and Computer Science, University of Ottawa, 800 King Edward Ave., Ottawa, Ontario, Canada*
[3]*Department of Physics, University of Ottawa, Ottawa, Ontario, Canada*
[4]*Centre for Research in Photonics at the University of Ottawa, Ottawa, Ontario, Canada*
[*]*berini@eecs.uottawa.ca*

Abstract: Single-mode distributed feedback laser structures and parity-time symmetry broken grating structures based on dielectric-loaded long-range surface plasmon polariton waveguides are proposed. The structures comprise a thin Ag stripe on an active polymer bottom cladding with an active polymer ridge. The active polymer assumed is PMMA doped with IR140 dye providing optical gain at near infrared wavelengths. Cutoff top ridge dimensions (thickness and width) are calculated using a finite element method and selected to guarantee single-mode operation of the laser. Several parameters such as the threshold number of periods and the lasing wavelength are determined using the transfer matrix method. A related structure based on two pairs of waveguides of two widths, which have the same imaginary part but different real part of effective index, arranged within one grating period, is proposed as an active grating operating at the threshold for parity-time symmetry breaking (*i.e.*, operating at an exceptional point). Such "exceptional point" gratings produce ideal reflectance asymmetry as demonstrated via transfer matrix computations.

OCIS codes: (250.5403) Plasmonics; (250.4480) Optical amplifiers; (230.7370) Waveguides.

References and links

1. M. S. Tame, K. R. McEnery, Ş. K. Özdemir, J. Lee, S. A. Maier, and M. S. Kim, "Quantum plasmonics," Nat. Phys. **9**(6), 329–340 (2013).
2. H. A. Atwater and A. Polman, "Plasmonics for improved photovoltaic devices," Nat. Mater. **9**(3), 205–213 (2010).
3. M. Mansuripur, A. R. Zakharian, A. Lesuffleur, S.-H. Oh, R. J. Jones, N. C. Lindquist, H. Im, A. Kobyakov, and J. V. Moloney, "Plasmonic nano-structures for optical data storage," Opt. Express **17**(16), 14001–14014 (2009).
4. P. Berini, "Plasmon-polariton waves guided by thin lossy metal films of finite width: bound modes of symmetric structures," Phys. Rev. B **61**(15), 10484–10503 (2000).
5. P. Berini, "Long-range surface plasmon polaritons," Adv. Opt. Photonics **1**, 484–588 (2009).
6. I. De Leon and P. Berini, "Amplification of long-range surface plasmons by a dipolar gain medium," Nat. Photonics **4**(6), 382–387 (2010).
7. E. K. Keshmarzi, R. N. Tait, and P. Berini, "Long-range surface plasmon single-mode laser concepts," J. Appl. Phys. **112**(6), 063115 (2012).
8. O. Krupin, H. Asiri, C. Wang, R. N. Tait, and P. Berini, "Biosensing using straight long-range surface plasmon waveguides," Opt. Express **21**(1), 698–709 (2013).
9. Y. H. Joo, S. H. Song, and R. Magnusson, "Demonstration of long-range surface plasmon-polariton waveguide sensors with asymmetric double-electrode structures," Appl. Phys. Lett. **97**(20), 201105 (2010).
10. T. Holmgaard, J. Gosciniak, and S. I. Bozhevolnyi, "Long-range dielectric-loaded surface plasmon-polariton waveguides," Opt. Express **18**(22), 23009–23015 (2010).

#236926 Received 25 Mar 2015; revised 5 Jun 2015; accepted 16 Jul 2015; published 23 Jul 2015

11. J. S. Fakonas, H. Lee, Y. A. Kelaita, and H. A. Atwater, "Two-plasmon quantum interference," Nat. Photonics **8**(4), 317–320 (2014).
12. S. M. García-Blanco, M. Pollnau, and S. I. Bozhevolnyi, "Loss compensation in long-range dielectric-loaded surface plasmon-polariton waveguides," Opt. Express **19**(25), 25298–25311 (2011).
13. P. Berini and I. De Leon, "Surface plasmon–polariton amplifiers and lasers," Nat. Photonics **6**(1), 16–24 (2011).
14. C. M. Bender and S. Boettcher, "Real spectra in non-hermitian hamiltonians having PT symmetry," Phys. Rev. Lett. **80**(24), 5243–5246 (1998).
15. M. Kulishov, J. Laniel, N. Bélanger, J. Azaña, and D. Plant, "Nonreciprocal waveguide Bragg gratings," Opt. Express **13**(8), 3068–3078 (2005).
16. L. Feng, Y.-L. Xu, W. S. Fegadolli, M.-H. Lu, J. E. B. Oliveira, V. R. Almeida, Y.-F. Chen, and A. Scherer, "Experimental demonstration of a unidirectional reflectionless parity-time metamaterial at optical frequencies," Nat. Mater. **12**(2), 108–113 (2013).
17. E. K. Keshmarzi, R. N. Tait, and P. Berini, "Spatially nonreciprocal Bragg gratings based on surface plasmons," Appl. Phys. Lett. **105**(19), 191110 (2014).
18. S. Longhi, "PT-symmetric laser absorber," Phys. Rev. A **82**(3), 031801 (2010).
19. V. V. Konotop, V. S. Shchesnovich, and D. A. Zezyulin, "Giant amplification of modes in parity-time symmetric waveguides," Phys. Lett. A **376**(42-43), 2750–2753 (2012).
20. H. Benisty, A. Degiron, A. Lupu, A. De Lustrac, S. Chénais, S. Forget, M. Besbes, G. Barbillon, A. Bruyant, S. Blaize, and G. Lérondel, "Implementation of PT symmetric devices using plasmonics: principle and applications," Opt. Express **19**(19), 18004–18019 (2011).
21. A. Regensburger, C. Bersch, M.-A. Miri, G. Onishchukov, D. N. Christodoulides, and U. Peschel, "Parity-time synthetic photonic lattices," Nature **488**(7410), 167–171 (2012).
22. B. Peng, S. K. Özdemir, S. Rotter, H. Yilmaz, M. Liertzer, F. Monifi, C. M. Bender, F. Nori, and L. Yang, "Loss-induced suppression and revival of lasing," Science **346**(6207), 328–332 (2014).
23. B. Peng, S. K. Ozdemir, F. Lei, F. Monifi, M. Gianfreda, G. L. Long, S. Fan, F. Nori, C. M. Bender, and L. Yang, "Parity–time-symmetric whispering-gallery microcavities," Nat. Phys. **10**(5), 394–398 (2014).
24. S. Jetté-Charbonneau, R. Charbonneau, N. Lahoud, G. A. Mattiussi, and P. Berini, "Bragg gratings based on long-range surface plasmon-polariton waveguides : comparison of theory and experiment," IEEE J. Quantum Electron. **41**(12), 1480–1491 (2005).
25. E. K. Keshmarzi, R. N. Tait, and P. Berini, "Near infrared amplified spontaneous emission in a dye-doped polymeric waveguide for active plasmonic applications," Opt. Express **22**(10), 12452–12460 (2014).
26. P. Yeh, *Optical Waves in Layered Media* (Wiley, 1988).
27. B. Ghamsari, A. Olivieri, F. Variola, and P. Berini, "Enhanced Raman scattering in graphene by plasmonic resonant Stokes emission," Nanophotonics **3**(6), 363–371 (2014).
28. A. Guo, G. J. Salamo, D. Duchesne, R. Morandotti, M. Volatier-Ravat, V. Aimez, G. A. Siviloglou, and D. N. Christodoulides, "Observation of PT-symmetry breaking in complex optical potentials," Phys. Rev. Lett. **103**(9), 093902 (2009).
29. M. Kulishov, B. Kress, and R. Slavík, "Resonant cavities based on parity-time-symmetric diffractive gratings," Opt. Express **21**(8), 9473–9483 (2013).

1. Introduction

Surface plasmon polaritons (SPPs) are evanescent electromagnetic waves coupled to free electrons at the surface of a metal. SPPs have a field maximum at the interface between the dielectric and metal, and are strongly confined to the interface [1]. SPPs have been widely studied for applications to, *e.g.*, photovoltaic cells [2], data storage [3], and waveguide structures [4] due to their interesting properties. However, SPPs generally have a short propagation length because of the strong confinement to the metal surface. For application to waveguide-based optical structures, long-range SPPs (LRSPPs) guided along a thin metallic stripe bounded symmetrically by dielectric materials are more suitable because of their lower propagation loss [5]. Many optical devices operating with LRSPPs on stripes have been reported [5], including recently, amplifiers [6], single-mode laser concepts [7] and optical biosensors [8,9].

Structuring the top dielectric in a dielectric-metal-dielectric structure produces lateral confinement - such a structure may still support LRSPPs and is referred to as a dielectric-loaded LRSPP (DL-LRSPP) waveguide [10,11]. Typically, DL-LRSPP waveguides are composed of a top dielectric ridge patterned on a thin metal film on a dielectric substrate. Key advantages of the DL-LRSPP waveguides are low propagation loss and ease of fabrication. Also the dielectric regions can be comprised of an optical gain material such as an organic dye-doped polymer, so they have potential as active optical devices [12,13].

#236926 Received 25 Mar 2015; revised 5 Jun 2015; accepted 16 Jul 2015; published 23 Jul 2015

In the field of quantum mechanics, much research has been carried out on parity and time symmetric (PTS) Hamiltonian systems after it was shown that they can have purely real eigenvalues even for non-Hermitian operators [14]. Complex potentials obeying the PTS condition are required for realizing a PTS Hamiltonian. In the field of optics, complex potentials can be realized by employing complex refractive indices representing optical gain or loss, so it is possible in principle to realize a PTS system. Optical PTS systems require that the complex refractive index obeys the condition that the real part of the refractive index must be an even function of position whereas the imaginary part must be odd. Moreover, to clearly observe interesting optical behavior due to a PTS refractive index distribution, it is necessary to ensure a balanced distribution of the real and imaginary modulation of complex refractive index, enabling operation at the so-called parity-time symmetry breaking point (also referred as an exceptional point). Many interesting phenomena, such as non-reciprocal wave propagation [15–17], coherent perfect absorption [18], and giant wave amplification [19] were reported based on this phenomenon. A theoretical discussion of PTS optical systems at the exceptional point based on plasmonics [20], the experimental realization of synthetic lattices using optical couplers [21], and micro-resonators [22,23] were also reported.

Plasmonic structures have intrinsic loss, which may be an advantage when applied to PTS systems because complex index modulation is necessary. In this paper, we propose two active step-in-width grating structures based on DL-LRSPP waveguides, leading to a novel single-mode distributed feedback (DFB) laser concept, and a PTS grating operating at an exceptional point, both at near-infrared wavelengths. The extraordinary behavior of the effective index of the fundamental mode of the DL-LRSPP waveguide as the width of the ridge is altered allows operation of the gratings at the exceptional point where ideal asymmetry is produced.

2. Active DL-LRSPP grating structures

Schematics of the suggested step-in-width grating structures are shown in Figs. 1(a) and 1(d); similar step-in-width gratings have been demonstrated as high-quality narrowband plasmonic reflectors for LRSPPs on metal stripe waveguides [24]. The DL-LRSPP waveguide is composed of a top ridge on a thin Ag stripe of finite width on a semi-infinite bottom cladding, as shown in in the cross-sectional view of Fig. 1(b). The thickness of the bottom dielectric layer should be large enough for it to be considered optically semi-infinite (> 5 μm). The thickness of the top ridge t_t, and the width of top ridge and Ag stripe, should be selected such that all TE modes and all higher-order TM modes are cut-off in order for the waveguide to operate as a single-mode structure. Details on the required dimensions are given in the next section. Typically t_{ag} affects the propagation loss of the LRSPP mode, so a smaller t_{ag} is better in order to have a larger gain in the laser structure. However, for the PTS grating structure, t_{ag} affects the balance of the complex refractive index, as will be discussed in Section 4, so it should be selected carefully. For these grating structures, organic dye material (IR140) which has optical gain at near-infrared wavelengths is assumed doped into poly-methylmethacrylate (PMMA) and selected as the dielectric material for the top ridge and bottom cladding of the DL-LRSPP waveguide; these regions are shown in purple in Fig. 1. The IR140-doped PMMA provides optical gain over the 850 – 900 nm wavelength range when pumped by a pulsed laser near 810 nm [25]. The thin Ag stripe, shown in gray in Fig. 1, has the same width as the top ridge. The active DL-LRSPP waveguide structure can be patterned into step-in-width gratings of period Λ_i (i = g or PT) with N_i periods leading to a DFB laser structure as sketched in Figs. 1(a) and 1(c), or a PTS grating structure as sketched in Figs. 1(d) and 1(e). For the DFB laser, we require two widths within one period (w_{gj}, j = 1, 2) carefully selected to produce low propagation losses. For the PTS grating, we require four widths (w_k, k = 1 - 4) within one period to form the even-function spatial distribution of the real part of effective index and the odd-function spatial distribution of the imaginary part of effective index.

#236926 Received 25 Mar 2015; revised 5 Jun 2015; accepted 16 Jul 2015; published 23 Jul 2015

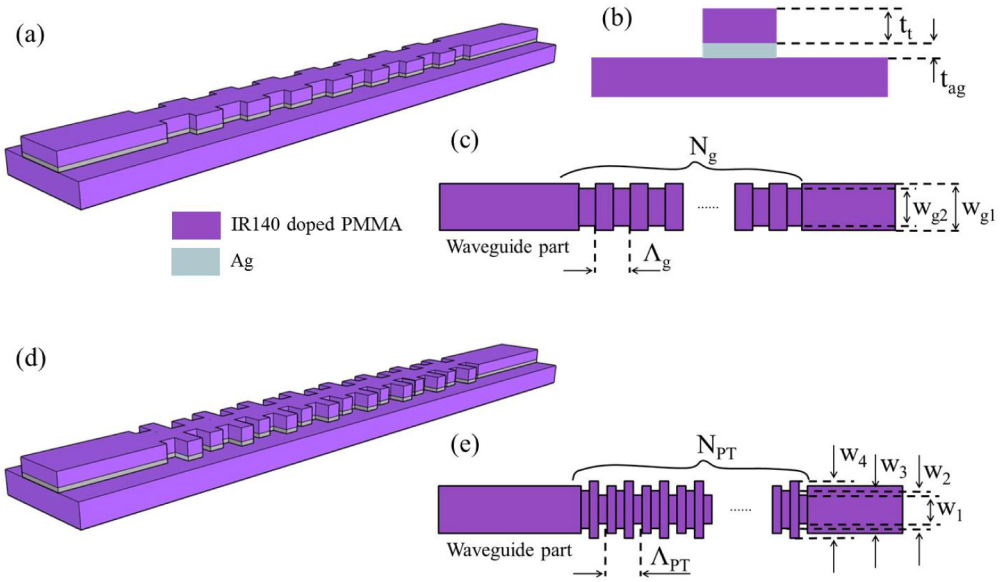

Fig. 1. (a) 3D view of a DFB laser structure. (b) Cross sectional view of the DL-LRSPP waveguide. (c) Top view of a DFB laser structure. (d) 3D view and (e) top view of a PTS grating structure.

3. Single mode distributed feedback laser

The real part (n_R) and imaginary part (n_I) of the effective refractive index of the first two DL-LRSPP waveguide modes were calculated using the finite element method as a function of the top ridge width for the passive case (no material gain) at a free-space operating wavelength of λ_0 = 880 nm, and are plotted in Fig. 2(a) as solid curves. In the calculations, t_{ag} = 25 nm thick Ag and a top ridge t_t = 950 nm thick were selected. The propagation loss of the guided modes is affected by t_{ag}, so for a DFB laser, a thinner t_{ag} is advantageous. Here we choose t_{ag} = 25 nm bearing in mind fabrication constraints which place a lower limit on the thickness of a Ag film to about this value. t_t was determined from the calculation of cutoff thickness of the TE modes. All TE modes can be cut-off by controlling t_t and the width of the ridge. Figure 2(b) shows the cutoff thicknesses for some cases of ridge width. For a 4 μm wide ridge, the cutoff thickness is 980 nm so we choose t_t = 950 nm (we will work with ridges that are about 4 μm wide). Also, to achieve a single-mode waveguide, the width should be selected narrower than the cutoff width of higher-order TM modes. The red curves in Fig. 2(a) correspond to the effective index of the ss_b^0 mode (fundamental LRSPP mode) and the black ones to the as_b^2 mode (first higher-order LRSPP mode) - see Ref [3]. for the mode nomenclature. The solid curves are for the passive case (no material gain in the PMMA) and the dashed curves are for the active case assuming 67 cm^{-1} of material gain in the PMMA [20]. The cutoff width of the as_b^2 mode is ~4.5 μm, so the DL-LRSPP structure can be single-LRSPP-moded by choosing the width and thickness of the top ridge as selected.

#236926 Received 25 Mar 2015; revised 5 Jun 2015; accepted 16 Jul 2015; published 23 Jul 2015

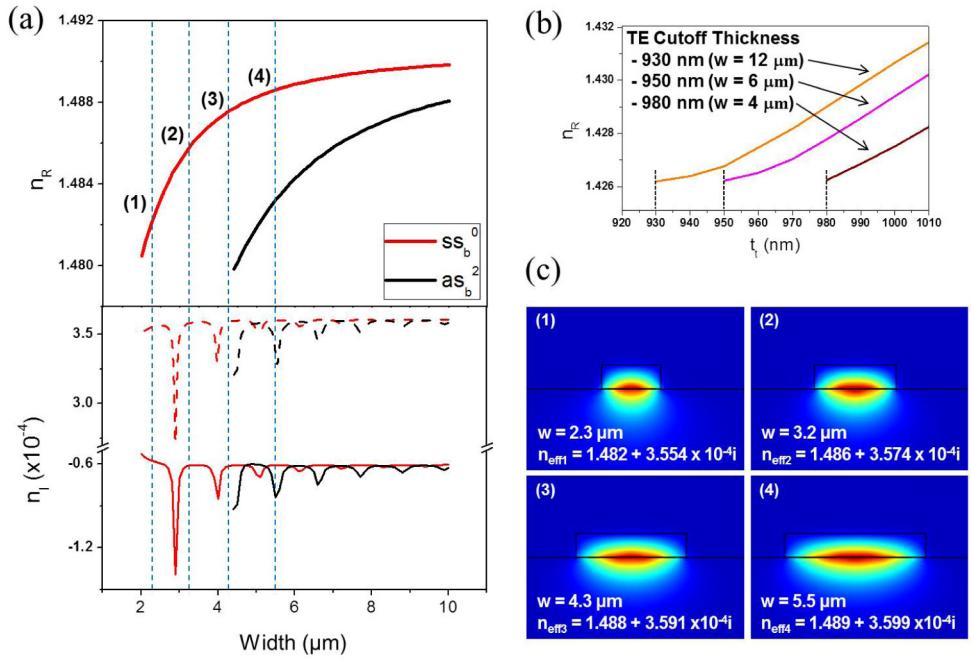

Fig. 2. (a) Effective index as function of the ridge width of the DL-LRSPP waveguide for a 25 nm thick Ag stripe and a 950 nm thick ridge. Red curves represent effective indices for ss_b^0 mode and black curves are for as_b^2 mode. The solid curves are for the passive case and the dashed curves for the active case (67 cm^{-1} of material gain for IR140-doped PMMA). (b) TE mode cutoff thickness of top ridge. (c) Mode profiles for widths having a low propagation loss.

There are some large dips in n_I, as observed in the bottom panel of Fig. 2(a), due to changes in the supermode character as different constituent SPP modes couple in and out of the supermode (modes in DL-LRSPP waveguides are supermodes formed by the coupling of constituent SPPs as in metal stripe waveguides [3]). However, the losses can be compensated by introducing material gain in the adjacent dielectric parts, as shown by the dashed curves in the bottom panel of Fig. 2(a). Also we can choose several candidate widths which produce low loss and that can be selected to form a DFB laser with a well-defined mode profile. For example, we choose four candidate widths as 2.3, 3.2, 4.3 and 5.5 μm marked by vertical dashed lines labelled 1 to 4 in Fig. 2(a). The candidate widths 1 to 3 are narrower than the cutoff width of the as_b^2 mode so the structure will be single-LRSPP-mode. Candidate width 4 can support the as_b^2 mode, however, it will be suppressed due to gain competition with the ss_b^0 mode because its propagation loss is larger. The n_I of the candidate widths are all near -6×10^{-4} (the minus sign implies propagation loss) but they can become positive ($\sim3.5\times10^{-4}$) with 67 cm^{-1} of material gain in both the top ridge and the bottom cladding (67 cm^{-1} of material gain has been measured for IR140-doped PMMA [25]). All widths thus have ~50 cm^{-1} of modal (LRSPP) gain. Figure 2(c) shows the mode profiles for the candidate widths and their effective index for the active case. The candidate width 3 was selected as the width for the waveguide (*i.e.*, as w_{g1} in Fig. 1(c)) because it has a small propagation loss and the waveguide is single-mode; the other widths are selected as the perturbed widths (*i.e.*, as w_{g2} in Fig. 1(c)).

The three combinations of the candidate widths, *i.e.*, w_{g1} = 4.3 μm with w_{g2} = 2.3, 3.2 and 5.5 μm, were considered and are denoted Set 1, Set 2 and Set 3, respectively. The operating (lasing) wavelength was selected to be near λ_0 = 880 nm because the gain material chosen provides maximum material gain around that wavelength. The grating pitch can be obtained as $\Lambda_g = O\lambda_0/2n_{ave}$ where O is the order of the grating, n_{ave} is average effective index within

#236926 Received 25 Mar 2015; revised 5 Jun 2015; accepted 16 Jul 2015; published 23 Jul 2015

one period taken as $n_{ave} = \mathrm{Re}\{n_{eff1} + n_{eff2}\}/2$, where n_{effj} is the effective index of a waveguide section of width w_{gj} (j = 1,2). The order of the grating was selected as 3rd because the grating period is then easier to fabricate although it leads to a longer structure than if 1st order gratings were selected. The physical dimensions of the proposed DFB lasers (widths and period) are realizable using, *e.g.,* e-beam lithography. Also the designed t_{ag} = 25 nm is easy to fabricate by, *e.g.*, metal evaporation.

The lasing properties were determined via the transfer matrix method (TMM) [26]. The threshold number of pitches ($N_{g,th}$) can be obtained by finding the value of N_g that makes the denominator of the transfer matrix zero. The lasing wavelength was obtained by computing the reflectance/transmittance spectra for $N_{g,th}$ periods. The DFB laser designs obtained, including $N_{g,th}$ for the 1st and 2nd lasing modes (longitudinal), their lasing wavelengths, and the difference in n_R (Δn_R) within one period are listed in Table 1.

Table 1. Threshold number of pitches and lasing wavelength of DFB laser designs.

	λ_0	Λ_g 3rd	1st lasing mode		2nd lasing mode		Δn_R
	[nm]	[nm]	$N_{g,th}$ 3rd	Lasing λ [nm]	$N_{g,th}$ 3rd	Lasing λ [nm]	
Set 1	880	888.9	492	$\lambda_0 \pm 0.607$	682	$\lambda_0 \pm 0.886$	0.005
Set 2		887.9	776	$\lambda_0 \pm 0.321$	994	$\lambda_0 \pm 0.566$	0.002
Set 3		887.1	990	$\lambda_0 \pm 0.230$	1206	$\lambda_0 \pm 0.456$	0.001

4. Parity time symmetry broken gratings

4.1 Supermode character of DL-LRSPP modes

In optics, PTS demands that the complex refractive index should obey the condition $n(\mathbf{r}) = n^*(-\mathbf{r})$, which means that n_R must have an even-function spatial distribution whereas n_I must have an odd-function spatial distribution. To achieve this condition with step-in-width gratings, we need four widths within one period which satisfy following conditions:

$$\begin{aligned} &\mathrm{Re}\{n_1\} = \mathrm{Re}\{n_3\} \neq \mathrm{Re}\{n_2\} = \mathrm{Re}\{n_4\}, \\ &\mathrm{Im}\{n_1\} = \mathrm{Im}\{n_4\} \neq \mathrm{Im}\{n_2\} = \mathrm{Im}\{n_3\}. \end{aligned} \tag{1}$$

In the above, n_k are complex effective indices of the ss_b^0 mode for waveguide segments of width w_k in Fig. 1(e). Thus we need two pairs of widths which have same n_I but different n_R. If we can find those pairs, we can satisfy the PTS distribution of complex refractive index ($n(\mathbf{r}) = n^*(-\mathbf{r})$) by arranging those widths in a specific sequence. The supermode character of the ss_b^0 mode in the DL-LRSPP waveguide makes it possible to find four widths which satisfy the above conditions. It is thus possible to form a grating structure which satisfies the PTS distribution of complex refractive index.

The effective index computed as a function of width in the passive case is shown in Fig. 3(a) for t_{ag} = 30 nm (it is difficult to find widths that satisfy Eq. (1) for thinner t_{ag}). The black curves for n_R and n_I in Fig. 3(a) correspond to the effective index of the ss_b^0 mode, and the colored curves are for higher-order highly-confined and high-loss asymmetric modes. The insets to Fig. 3(a) give the corresponding mode profiles. Of particular interest are the crossings in n_R between the asymmetric modes and the ss_b^0 mode.

The supermode character of the ss_b^0 mode is apparent as it couples (hybridizes) with some of the asymmetric modes near crossings in n_R. The coupling width is slightly wider than the cutoff width of the asymmetric modes, marked with vertical red dashed lines in Fig. 3(a). Figures 3(b) to 3(d) show expanded views near the black dashed circles in Fig. 3(a), *i.e*., near the regions of n_R crossings of the ss_b^0 mode with the sa_b^3, aa_b^4 and sa_b^5 modes. The sa_b^3 and sa_b^5 modes share the same vertical symmetry as the ss_b^0 mode, so they couple (hybridise) near their crossings in n_R, as shown in Figs. 3(b) and 3(d). As they couple, their field distribution is perturbed, as is apparent from the plots in inset, and n_R oscillates as the width changes. It is the peculiar behavior of n_R and n_I with width, near the n_R crossing of the ss_b^0 and sa_b^3 modes,

#236926 Received 25 Mar 2015; revised 5 Jun 2015; accepted 16 Jul 2015; published 23 Jul 2015

that enables a PTS grating, as will be discussed below (the other crossing with the sa_b^5 mode produces perturbations that are a bit too weak).

As the ss_b^0 mode couples to an asymmetric mode, its propagation loss increases due to the higher loss of the latter, and conversely, the loss of the corresponding asymmetric mode decreases, as is apparent from the bottom panel of Fig. 3(a).

The aa_b^4 mode does not share the same vertical symmetry as the ss_b^0 mode so it does not couple at the n_R crossing, as is evident from Fig. 3(c) and the field plot in inset, and from the lower panel of Fig. 3(a) (*i.e.*, n_I is unperturbed at the n_R crossing).

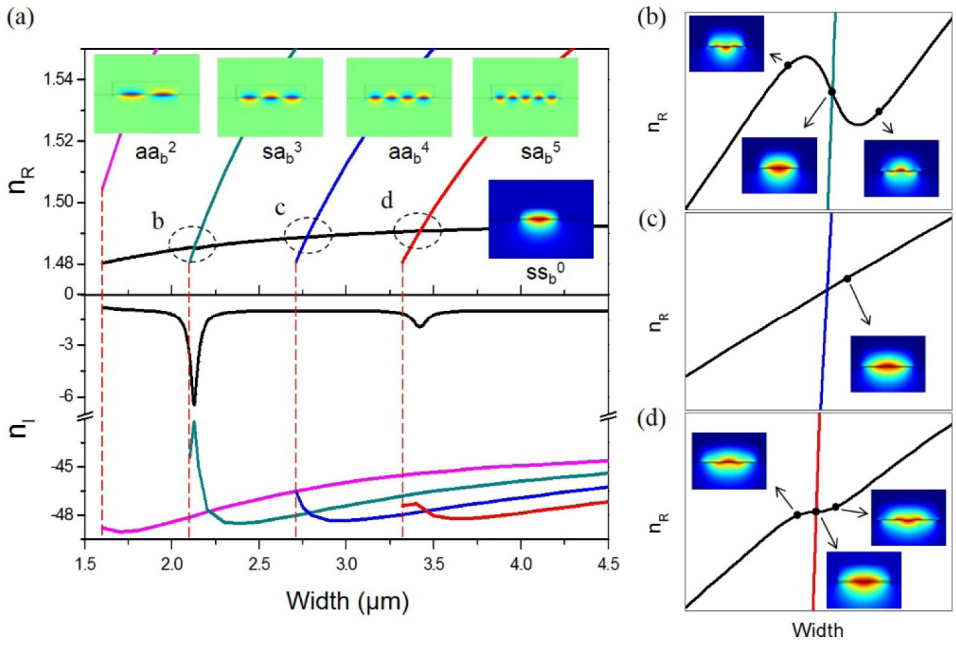

Fig. 3. (a) Effective index as function of width of the ss_b^0 mode and several asymmetric modes in a DL-LRSPP waveguide with a 30 nm thick Ag stripe. Vertical red dashed lines indicate cutoff widths for each mode and the figures in inset show the mode profile of each mode. (b-d) Expanded plots for the range marked with black dashed circles in Fig. 3(a). The insets of (b-d) are mode profiles for the widths marked with a black dot.

4.2 Balanced PTS distribution of complex refractive index

The PTS grating requires four widths as shown in Fig. 1(e) (w_k, k = 1 - 4), to achieve an even spatial distribution for n_R and an odd spatial distribution for n_I. To satisfy this condition, we need to find four widths satisfying the constraints of Eq. (1). Normally in a typical waveguide it is impossible to achieve this because both n_R and n_I change monotonically with geometry. However, in the DL-LRSPP waveguide, it is possible to find widths around n_R crossings, for instance, where the ss_b^0 and sa_b^3 modes couple, that produce effective indices that satisfy Eq. (1), because n_R and n_I do not vary monotonically in this region; a large dip for n_I and a local peak then a dip for n_R are observed in Fig. 3(b). Thus it is possible to find an arrangement of widths which allow a PTS distribution of complex refractive index.

In Fig. 4(a), n_R and n_I are re-plotted in expanded view over the n_R crossing region, for clarity. We can select the widths at the local peak and dip in n_R, denoted w_2 and w_3, on Fig. 4(a). In this case, we have different n_R values but equal n_I values because the dip in n_I occurs between the peak and dip in n_R. Also we can select w_1 and w_4 as shown, which again produces equal n_I values, but n_R values that are now equal to those produced by w_3 and w_2, respectively. Now, by arranging the widths within one grating period as shown in Fig. 4(b), in the sequence

#236926 Received 25 Mar 2015; revised 5 Jun 2015; accepted 16 Jul 2015; published 23 Jul 2015

w_3, w_2, w_4, w_1, we satisfy Eq. (1), and thus produce a PTS broken distribution of complex refractive index (*i.e.*, the condition $n(\mathbf{r}) = n^*(-\mathbf{r})$ is satisfied about the bisector of each period, taken at the junction of the sections of width w_2 and w_4). The red curve in Fig. 4(b) pertains to the n_R distribution and the blue curve pertains to the n_I distribution within one grating period. The length of each section of width w_k is set to a quarter period, $\Lambda_{PT}/4$. The dimensions of the sections within a period (steps in width of ~30 nm) are realizable using a high-resolution patterning method such as e-beam lithography [27].

The results of Fig. 4 were obtained in the passive case; *i.e.*, the gain of IR140-doped PMMA was not included. It would be desirable to introduce optical gain to make the average value of n_I zero or positive, thus producing better performance. Introducing gain to offset the average value of n_I does not alter the design in principle, because this corresponds to a gauge transformation [28].

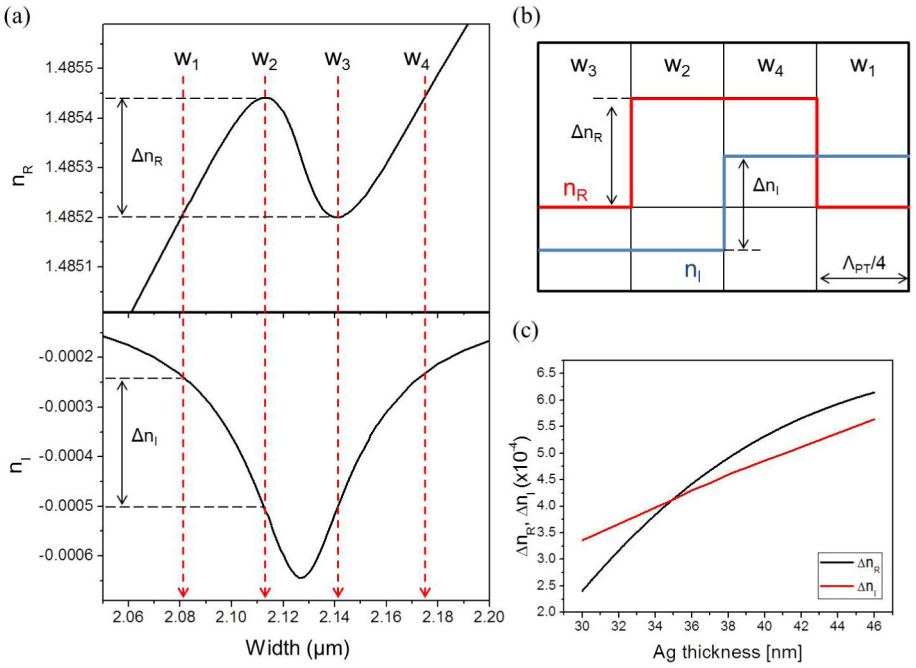

Fig. 4. (a) Real and imaginary part of effective index near the n_R crossing region of the ss_b^0 and sa_b^3 modes. Vertical red dashed lines indicate four widths selected for a PTS grating. (b) Schematic of the real and imaginary index distribution within one period. (c) Index difference as a function of Ag thickness.

Another important condition for a PTS grating structure is the balance between Δn_R, the difference in n_R, and Δn_I, the difference in n_I. Typically extraordinary behavior appears around the balance point (*i.e.* $\Delta n_R = \Delta n_I$), which corresponds to the PTS breaking point (*i.e.*, the threshold for parity-time symmetry breaking or the exceptional point). Exceptional optical properties engendered by a PTS index distribution are not evident when the balance between Δn_R and Δn_I is destroyed (even if the structure satisfies the PTS distribution of complex refractive index). But our proposed grating structure can have an exactly balanced index modulation by controlling t_{ag}, leading to grating operation at the threshold for PTS breaking (exceptional point). Consequently, the proposed PTS broken grating structure should have a maximally asymmetric reflectance at the balance point. The index differences as a function of t_{ag} are plotted in Fig. 4(c) from which the balance point can be identified: $\Delta n_R = \Delta n_I$ for t_{ag} = 35 nm (*i.e.*, the balance point can be obtained by careful adjustment of t_{ag}).

#236926 Received 25 Mar 2015; revised 5 Jun 2015; accepted 16 Jul 2015; published 23 Jul 2015

The PTS broken grating was also assumed to be of 3rd order and the Bragg wavelength was selected to be 880 nm for the same reasons as in the DFB case. N_{PT} was taken to be 1000. The reflectance spectra from the left side (R_l) and from the right side (R_r) for t_{ag} = 35 nm is shown in Fig. 5(a) for the passive case. We note a reflection from the left side but not from the right, so the reflectance is clearly asymmetric. The reflection port R_l has a low reflectance because the structure is passive and there is loss. Figure 5(b) shows the reflectance from each port at 880 nm as a function of the material gain in the PMMA regions. By increasing the gain, which means increasing the optical pumping power in a real experiment, R_l increases, eventually becoming larger than 1 for a material gain of about 40 cm^{-1}, whereas R_r remains near zero. R_l would increase more rapidly with gain by increasing N_{PT}. The amount of optical gain considered in Fig. 5(b) is realizable in IR140-doped PMMA [25]. The effective index differences Δn_R and Δn_I change slightly as the material gain increases, and thus so does the balance, which is the reason why R_r grows slightly beyond 60 cm^{-1} of material gain. This could be corrected by adjusting t_{ag} for operation with a prescribed amount of material gain.

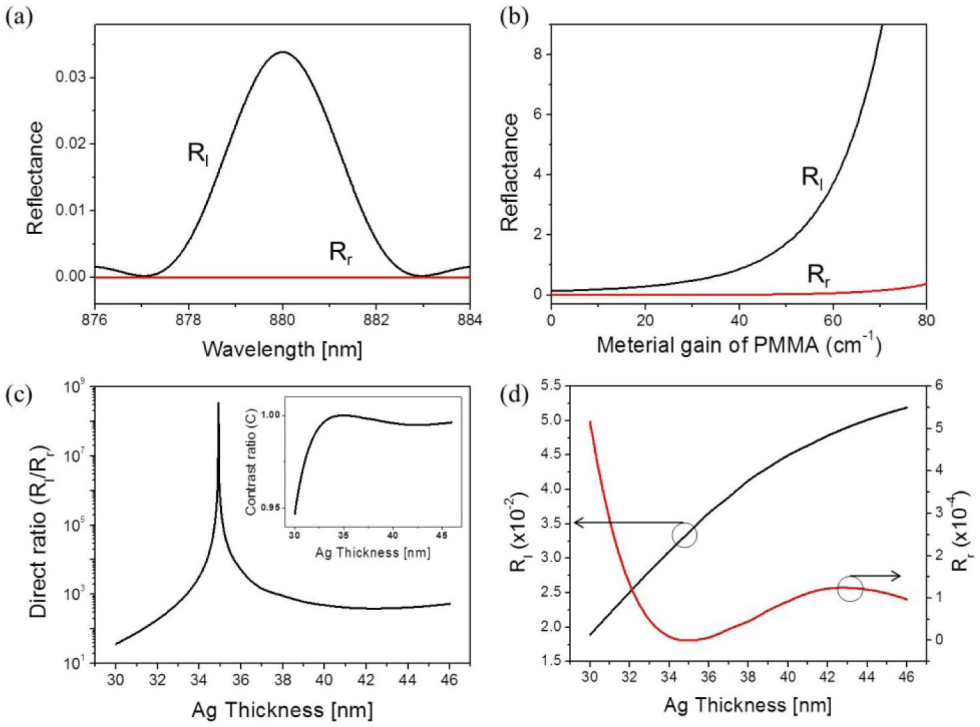

Fig. 5. (a) Reflectance from the left side R_l and the right side R_r of a passive PTS grating operating at the exceptional point. (b) Reflectance at 880 nm from the left and right sides as a function of material gain. (c) Direct and contrast ratio computed from the passive reflectances. (d) Left and right passive reflectances at 880 nm.

Figure 5(c) shows the direct ratio and the contrast ratio (C) of the passive R_l to R_r at 880 nm as a function of Ag thickness. The contrast ratio is defined as $C = (R_l-R_r)/(R_l + R_r)$ and is helpful to characterise the degree of asymmetry. The direct ratio has its maximum at t_{ag} = 35 nm, which corresponds to the balance point as shown in Fig. 4(c). This strong peak originates from the decrease of R_r as shown in Fig. 5(d) as the red curve, whereas R_l shown as the black curve in Fig. 5(d) increases smoothly which is typical of a grating when the effective index increases. However, even though there is a strong peak in the direct ratio at the balance point, C remains close to 1 over the whole range of t_{ag} considered. So the asymmetric reflectance property is sufficiently tolerant to variations in t_{ag} for practical fabrication.

#236926 Received 25 Mar 2015; revised 5 Jun 2015; accepted 16 Jul 2015; published 23 Jul 2015

The proposed PTS broken grating is similar in construction to the DFB laser of the previous section. However, the PTS broken grating cannot oscillate because, as shown in Fig. 5(a), it does not reflect light from one side; this is due to the lack of contra-directional coupling which also inhibits the optical feedback necessary for oscillation. However a cavity can be formed by concatenating two PTS broken gratings with opposite non-reflective ends, and a gain waveguide placed within the cavity, to create a laser [29].

5. Conclusion

DL-LRSPP waveguides are easy to fabricate and can guide a LRSPP mode which has a low propagation loss. Two grating concepts implemented as step-in-width structures in this waveguide, a single-mode DFB laser and a PTS broken grating, were proposed and analyzed. For single-mode operation of the DFB laser structure, t_t should be thinner than the cutoff thickness of all TE modes and the ridge width should be narrower than the cutoff width of the first higher-order LRSPP mode. Several candidate designs were proposed as DFB laser structures, and laser parameters such as the threshold number of periods and the lasing wavelength were calculated. Features in n_R and n_I curves as a function of ridge width, due to the coupling of the fundamental LRSPP with a high-order asymmetric mode, were observed and exploited to satisfy the constraints for a PTS grating structure. By arranging four waveguide segments of four different widths within one grating period, the complex refractive index distribution required for PTS broken gratings was obtained. Asymmetric reflectance spectra were computed which is a well-known property of a PTS broken grating structure. Ideal (reflectionless) asymmetry was observed for a design that produced $\Delta n_R = \Delta n_I$, corresponding to operation at the PTS breaking (exceptional) point, but asymmetric operation was observed over a large range of t_{ag} (30 – 45 nm), which is an advantage from the fabrication point of view because it means that the designs are tolerant to fabrication imperfections in the Ag thickness.

Acknowledgments

Useful discussions with Anthony Olivieri and Elham Karami Keshmarzi are gratefully acknowledged. This research was supported by Global Frontier Program through the National Research Foundation of Korea (NRF) funded by the Ministry of Science, ICT & Future Planning (NRF-2014M3A6B3063708).

#236926 Received 25 Mar 2015; revised 5 Jun 2015; accepted 16 Jul 2015; published 23 Jul 2015